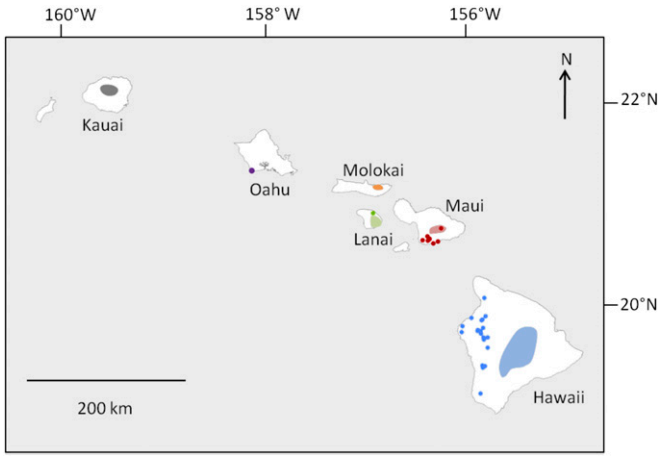

Fig. 1. Collection sites for Hawaiian petrel subfossil bones (dark-colored points), historic breeding distribution for the potentially extirpated population on Molokai, and modern breeding distribution on Kauai, Lanai, Maui, and Hawaii (lighter colored shapes). The distribution on Hawaii includes the saddle region between Mauna Kea and Mauna Loa, where Hawaiian petrel breeding is only documented by indigenous knowledge and bones (46, 58).

4,000 y, to well before human presence in the oceanic Northeast Pacific (3, 4). Our study therefore provides a unique, fishery-independent window into potential anthropogenic alterations of oceanic food webs.

Results and Discussion

We conducted a species-wide study of the Hawaiian petrel based on stable isotope data from six populations and two tissues: collagen and flight feather. Collagen is ideal for constructing long-term isotope chronologies, not only because it is preserved in ancient bones, but because its slow turnover rate in living birds results in an isotopic composition that can reflect foraging over a period of years (19). For the Hawaiian petrel, collagen data also provide spatially integrated dietary signals from individuals that are capable of traveling over large portions of the Northeast Pacific ocean, even within a single season (13). In contrast, flight feathers grow in a month or less during either the breeding season (for hatch-year birds) or nonbreeding season (for adults) (12, 15). Isotope data from flight feathers are therefore more useful for showing the diversity of foraging strategies present among Hawaiian petrels during short periods of time. Here, we study the isotopic composition of modern flight feathers to understand spatial and seasonal variation in petrel foraging habits and to aid in interpretation of our isotope chronologies from collagen.

We found large disparities in feather $\delta^{15}N$ and $\delta^{13}C$ values among populations and age groups, which we interpret as reflecting mainly divergences in foraging locations (Fig. 2, Table S1), as did Wiley et al. (15) in a study of two Hawaiian petrel populations. Our spatial interpretation of feather data is based on well-recognized $\delta^{15}N$ and $\delta^{13}C$ gradients within the Hawaiian petrel's distribution (Fig. 2*A*) (15), and is supported by observational studies. In brief, multiple data sets indicate that throughout North Pacific food webs, $\delta^{13}C$ varies inversely with latitude and $\delta^{15}N$ values decline precipitously away from an area of elevated $\delta^{15}N$ values in the southeast portion of Hawaiian petrel distribution, between 4–10° N and 135–140°W (20–24). Thus, petrels that focus their foraging southeast of the Hawaiian Islands are expected to have relatively high $\delta^{13}C$ and $\delta^{15}N$ values. Alternatively, the relatively high $\delta^{15}N$ values, such as those we observed for Lanai and Hawaii populations, could be due to feeding at a higher trophic level than other petrels. However, Laysan albatross (*Phoebastria immutabilis*) feeding north of the Hawaiian Islands, away from the region of elevated $\delta^{15}N$, have relatively low $\delta^{15}N$ values (12.5‰) (15). Because Hawaiian petrels are unlikely to forage at a higher trophic level than the related and substantially larger Laysan albatross, $\delta^{15}N$ values greater than 12.5‰ in Hawaiian petrel feathers must result from feeding in a region of elevated $\delta^{15}N$.

High $\delta^{13}C$ values among adults are consistent with all adults growing feathers in the southern portion of Hawaiian petrel distribution, with variable $\delta^{15}N$ indicating that populations rely to different extents on areas of elevated $\delta^{15}N$ (e.g., in the southeast portion of the species' distribution; Fig. 2*A*). Relatively low $\delta^{13}C$ values of Maui and Kauai hatch-year birds are consistent with parental foraging trips near and north of the Hawaiian Islands, as shown by satellite tracks from Maui petrels (Fig. 2). In contrast, petrels from Hawaii likely provision their chicks with prey from southeast of the Hawaiian Islands, based on the elevated $\delta^{15}N$ and $\delta^{13}C$ values in the feathers of Hawaii hatch-year birds. Our interpretations of feather data are supported by multiple observational studies. For example, petrels breeding on Hawaii visit their nests more frequently than petrels on Maui, presumably due to shorter foraging trips to different at-sea locations (12, 25). In addition, at-sea observations show that Hawaiian petrels are more concentrated to the southeast of the Hawaiian Islands from October to December (the late breeding season and early nonbreeding season) than during the midbreeding season, consistent with our interpretation that adult petrels move toward this area during the early nonbreeding season (14). Overall, feather data show substantial variation in foraging location, both seasonally and among populations. In contrast, neither $\delta^{15}N$ nor $\delta^{13}C$ values of bone collagen vary significantly among modern petrel populations (comparisons of collagen $\delta^{15}N$ among populations can be found in Table S2; ANOVA for $\delta^{13}C$, $P = 0.597$, $F = 0.8434$, df = 11). Isotopic signals of location are apparently averaged out in modern bone collagen, likely due to the long time period represented by this tissue and the extensive foraging range of individual birds over the course of the breeding and nonbreeding seasons, combined.

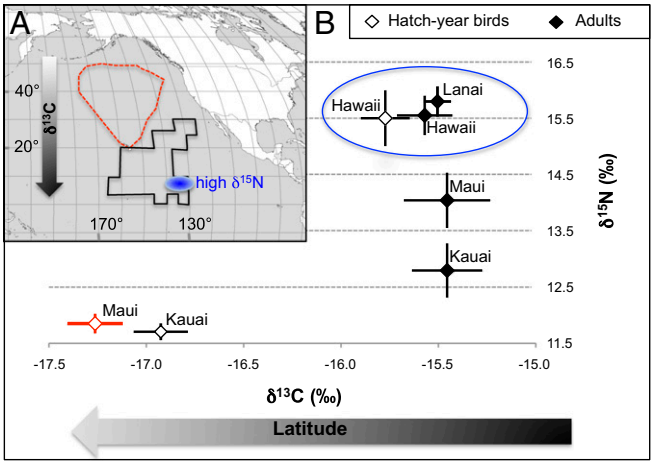

Fig. 2. Flight feather isotope data and at-sea locations of Hawaiian petrels. In *A*, the black line marks Hawaiian petrel distribution from transect surveys (14). The red dashed line is a typical flight path from a satellite-tracked Maui bird during the breeding season (13). These two regions represent the predominate areas where Hawaiian petrels occur. In *A*, the blue oval denotes an approximate area where organic matter and consumers have unusually high $\delta^{15}N$ values within the Hawaiian petrel's range (23, 24). In *B*, the blue circle identifies petrels that apparently concentrate their foraging in a region with elevated $\delta^{15}N$. In both panels, arrows emphasize the negative relationship between latitude and $\delta^{13}C$ of marine organisms (20–22). Hatch-year birds from Maui are outlined in red to associate them with the Maui flight path.

To evaluate temporal trends in foraging, we first grouped collagen samples into island populations: a grouping that allowed separate examination of genetically distinct populations with disparate foraging locations. Next, we divided collagen samples into time bins and compared average isotope values using ANOVA and Tukey honestly significant difference (HSD) post hoc tests (Fig. 3, Table S2). The initial time bins are based on archaeological chronology in the Hawaiian Islands, which were the population center for people fishing within the oceanic range of the Hawaiian petrel until historical times (in contrast, aboriginal people living on continents concentrated their fishing in nearshore environments of the continental shelves) (3, 5). The later time bins reflect the Historic period of Western economic development and whaling in Hawaii and the oceanic eastern North Pacific, followed by the Modern period of industrialized fishing.

Our isotope chronologies show that $\delta^{15}N$ disparities among populations have decreased through time. Before the Historic period, $\delta^{15}N$ values of bone collagen differ by as much as 2‰ and show statistically significant separation (Fig. 3, Table S2). In contrast, isotopic segregation is only observable among modern populations over the short time scales represented by flight feathers. This isotopic convergence of populations may be related to a seemingly concurrent, species-wide shift in $\delta^{15}N$ values.

Between the Prehuman and Modern periods, we observed significant $\delta^{15}N$ declines for petrel populations on Lanai, Maui, and Hawaii (all of the populations from which modern samples were available) (Fig. 3, Table S2). $\delta^{15}N$ values from the sample-rich Hawaii chronology did not decline until sometime after the early Expansion period ($P < 0.01$ for Expansion vs. Modern periods, $P = 0.44$ for Prehuman vs. Expansion periods). The 10 most recent Expansion period samples from Hawaii (average age = 204 B.P.) had an average $\delta^{15}N$ of 16.8 ± 0.5‰, which is similar to the average $\delta^{15}N$ of the remaining samples in this time period (16.5 ± 0.1‰) and implies that the $\delta^{15}N$ decline occurred after ca. 200 B.P. Petrels collected on the island of Molokai in 1914 have an average $\delta^{15}N$ value that does not differ significantly from that of any ancient population ($P = 0.072$ for Prehuman Hawaii, $P > 0.76$ for all other comparisons), but is higher than the $\delta^{15}N$ of modern Maui and Lanai populations (Table S2), suggesting that $\delta^{15}N$ decline occurred within the past 100 y. Notably, the decline in $\delta^{15}N$ between ancient and modern petrels is a robust characteristic of our timelines: it is present regardless of the time bins chosen for the ancient samples. Preceding the isotopic decline, a relative stasis in average $\delta^{15}N$ values is supported by results from the islands of Oahu, Hawaii, and Maui. When the Modern time bin is excluded, there is no decline in $\delta^{15}N$ for Maui or Hawaii (Table S2). Similarly, before its extirpation around 600 B.P. (615 B.P., youngest date), there is no change in $\delta^{15}N$ of the Oahu population ($P = 1.00$). Overall, our data support a recent, species-wide shift in $\delta^{15}N$ that was unprecedented during the last 4,000 y.

We considered whether anthropogenic impact to $\delta^{15}N$ through a North Pacific–wide input of isotopically unique nitrogen could have influenced our results. However, atmospheric deposition of ^{15}N-depleted anthropogenic nitrogen to the ocean and a possible increase in nitrogen fixation together cannot explain even a 0.2‰ decrease in $\delta^{15}N$ values (see modeling in *SI Text S1*). Additionally, we find no evidence that Hawaiian petrel $\delta^{13}C$ or $\delta^{15}N$ values vary with the El Niño Southern Oscillation or longer term climatic perturbations (*Materials and Methods*) (15). Furthermore, because all modern island populations have lower average $\delta^{15}N$ values than all ancient populations, migration among islands cannot explain the $\delta^{15}N$ decline. This conclusion is supported by genetic analyses, which show that migration was very low among islands before human colonization and is currently low among extant populations (17, 18).

We considered whether declining population size in the Hawaiian petrel could be causally linked with the observed isotopic shift. However, the timing of $\delta^{15}N$ decline argues against this explanation. Our analysis identifies the isotopic shift occurring most likely within the past 100 y. While the population trend over the past century is not well documented, the majority of population

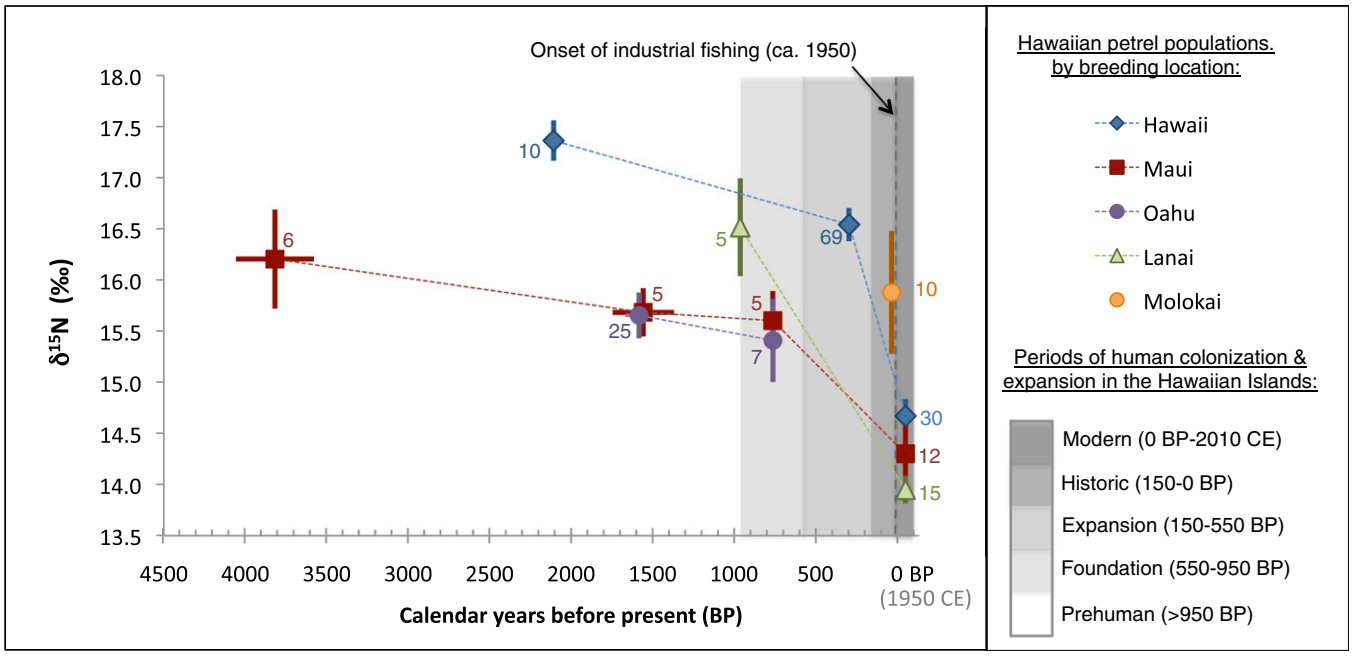

Fig. 3. $\delta^{15}N$ values of modern and radiocarbon-dated bone collagen for five Hawaiian petrel populations. The average age and isotopic composition of each time bin, ± SE, is plotted with sample size noted (see Fig. S1 for $\delta^{13}C$ results and Fig. S2 for confidence intervals of radiocarbon dates). Gray shading indicates time bins. Modern samples were unavailable from Oahu and Molokai due to population extirpation. Stippled lines connecting data points are for visualization purposes; isotopic shifts between time bins may have occurred nonlinearly. CE, Common Era.

compound bones (e.g., lacrimal incompletely fused to the neurocranium, suture between nasal bones extending farther anterior than in adults); bony surfaces, especially of the major wing bones, the tarsometatarsus, and the maxilla, are pitted and striated in places (Fig. S3); muscle impressions and growth zones may have a spongy texture; and there is a higher density of small nutrient foramina at the articular ends of some long bones. As the bird matures further, the boney surfaces become smoother and less vascularized. Among the most persistent signatures of a hatch-year bird are the higher density of small nutrient foramina on the proximal tarsometatarsus, the incomplete fusion of the lacrimals, and the spongy or rugose texture of fossa musculus brachialis on the humerus and impressio brachialis on the ulna. Some bones, such as the coracoid and femur, mature quickly and are not reliable for distinguishing older hatch-year birds from adults. These observations are based on the series of skeletons of Hawaiian petrel and Newell's shearwater in the skeleton collection of the National Museum of Natural History, Division of Birds, which includes numerous specimens of hatch-year birds that had already fledged at the time of death.

1. Sigman DM, Altabet MA, McCorkle DC, Francois R, Fischer G (2000) The δ15N of nitrate in the Southern Ocean: Nitrogen cycling and circulation in the ocean interior. *J Geophys Res* 105(C8):19599–19614.
2. Duce RA, et al. (2008) Impacts of atmospheric anthropogenic nitrogen on the open ocean. *Science* 320(5878):893–897.
3. Macko SA, Ostrom NE (1994) Pollution studies using stable isotopes. *Stable Isotopes in Ecology and Environmental Science*, eds Lajtha K, Michener RH (Blackwell, Boston), pp 45–62.
4. Karl D, et al. (1997) The role of nitrogen fixation in biogeochemical cycling in the subtropical North Pacific Ocean. *Nature* 388(6643):533–538.
5. Dore JE, Brum JR, Tupas LM, Karl DM (2002) Seasonal and interannual variability in sources of nitrogen supporting export in the oligotrophic subtropical North Pacific Ocean. *Limnol Oceanogr* 47(6):1595–1605.
6. Ruiz-Cooley RI, Villa EC, Gould WR (2010) Ontogenetic variation of $\delta^{13}C$ and $\delta^{15}N$ recorded in the gladius of the jumbo squid Dosidicus gigas: Geographic differences. *Mar Ecol Prog Ser* 399:187–198.
7. Parry M (2007) Trophic variation with length in two ommastrephid squids, Ommastrephes bartramii and Sthenoteuthis oualaniensis. *Mar Biol* 153(3):249–256.
8. Stergiou KI (2002) Overfishing, tropicalization of fish stocks, uncertainty and ecosystem management: Resharpening Ockham's razor. *Fish Res* 55:1–9.

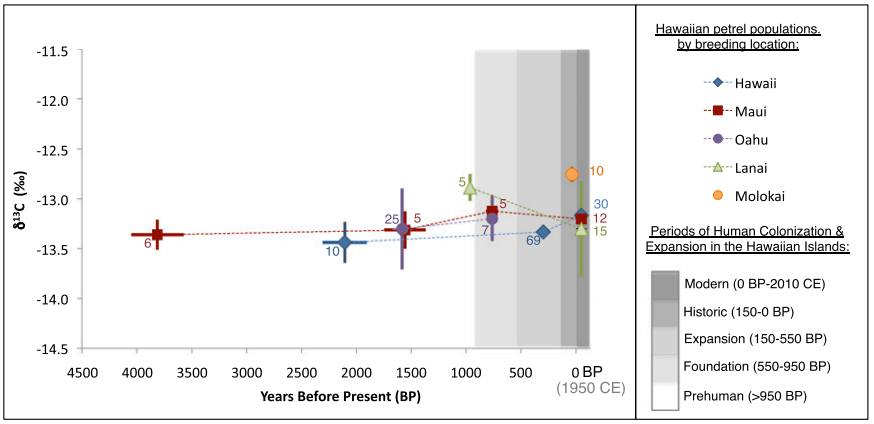

Fig. S1. Suess-corrected $\delta^{13}C$ values of modern and radiocarbon-dated bone collagen for five Hawaiian petrel populations. The average age and isotopic composition of each time bin, ±SE, is plotted with sample size noted. Gray shading indicates time bins. Modern samples were unavailable from Oahu and Molokai due to population extirpation. Stippled lines connecting data points are for visualization purposes; isotopic shifts between time bins may have occurred nonlinearly.

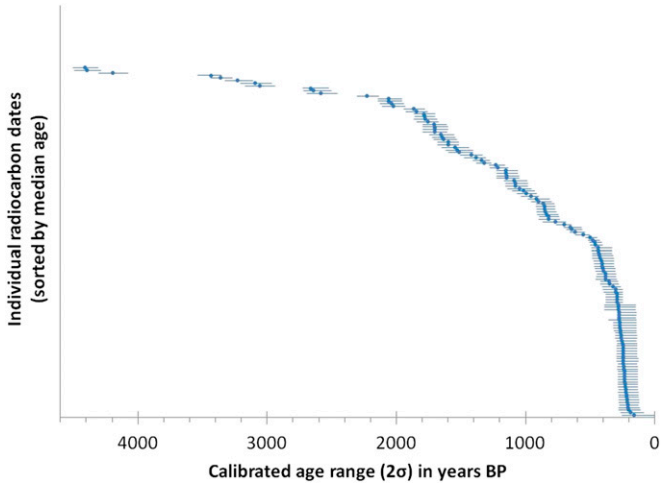

Fig. S2. The 95% confidence interval of 133 calibrated radiocarbon dates used in the present study (median ages marked by diamonds within confidence intervals).

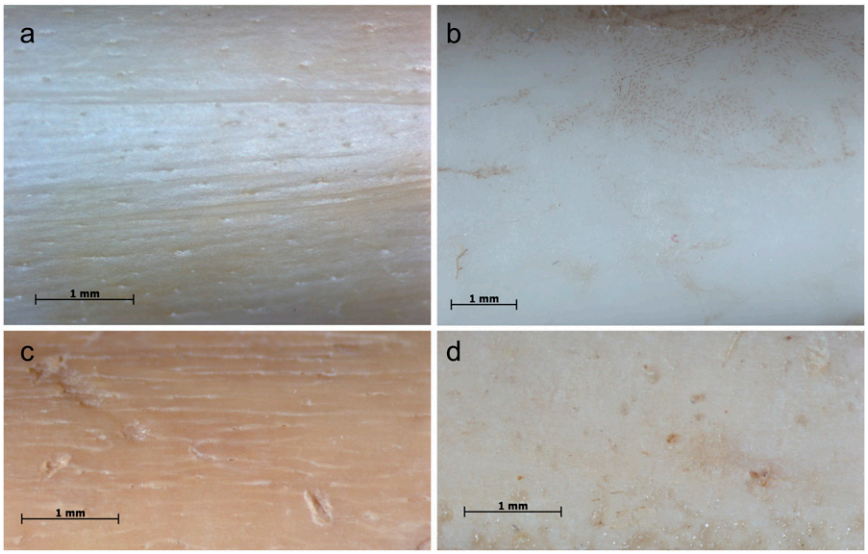

Fig. S3. Shafts of seabird humeri, illustrating one example of the observed differences in bone surface morphology between adult-sized hatch-year birds, and adults. (*A*) USNM 556797, a hatch-year Newell's shearwater; (*B*) USNM 639525, an adult Newell's shearwater; (*C*) MDS2005HY, a subfossil hatch-year Hawaiian petrel; and (*D*) MDS2005AD, a subfossil adult Hawaiian petrel. The hatch-year bones show pits and striations indicative of vascularization, whereas the adult bones show a smooth surface. Pictures taken with a Zeiss Axiocam attached to a Zeiss Stereo Discovery V12, and prepared with Zeiss AxioVision software to increase the depth of field.

Table S1. Tukey honestly significant difference post hoc comparisons for $\delta^{15}N$ (above diagonal) and $\delta^{13}C$ values (below diagonal) of Hawaiian petrel flight feathers

Island-age	Hawaii A	Hawaii HY	Lanai A	Maui A	Maui HY	Kauai A	Kauai HY
Hawaii A	—	1.000	0.999	0.071	<0.001*	<0.001*	<0.001*
Hawaii HY	0.992	—	0.999	0.272	<0.001*	<0.001*	<0.001*
Lanai A	0.999	0.910	—	0.009*	<0.001*	<0.001*	<0.001*
Maui A	0.999	0.999	1.000	—	0.006*	0.247	<0.001*
Maui HY	<0.001*	<0.001*	<0.001*	<0.001*	—	0.716	1.000
Kauai A	0.999	0.910	1.000	<0.001*	0.844	—	0.449
Kauai HY	<0.001*	<0.001*	<0.001*	<0.001*	0.844	<0.001*	—

P values are shown. Age classes are abbreviated as A (adult) and HY (hatch-year bird).
*Statistically significant difference ($\alpha = 0.05$).

Table S2. Tukey HSD post hoc comparisons for $\delta^{15}N$ values of Hawaiian petrel collagen

Island-Bin	Hawaii 3	Hawaii 4	Maui 1	Maui 4	Maui 5	Maui 6	Oahu 4	Oahu 5	Lanai 1	Lanai 4	Molokai 2
Hawaii 1	<0.01*	<0.01*	0.993	0.854	0.684	0.064	0.887	0.041	0.520	0.021*	0.090
Hawaii 3	—	0.441	<0.01*	0.661	0.843	1.000	0.219	0.020	<0.01*	1.000	0.768
Hawaii 4		—	<0.01*	0.037*	0.077	0.427	<0.01*	<0.01*	<0.01*	0.882	0.072
Maui 1			—	0.345	0.202	<0.01*	0.359	<0.01*	0.998	<0.01*	0.024*
Maui 4				—	1.00	0.990	1.000	1.000	0.065	0.893	1.000
Maui 5					—	0.999	1.000	1.000	0.028*	0.961	1.000
Maui 6						—	0.929	0.977	<0.01*	1.00	1.000
Oahu 4							—	1.000	0.050*	0.686	0.999
Oahu 5								—	<0.01*	0.769	1.000
Lanai 1									—	<0.01*	<0.01*
Lanai 4										—	0.993

P values are shown. Numbers refer to time bins, as defined in *Materials and Methods*, with 1 indicating the Modern time bin, or Modern Period, and moving backward in time, with 5 indicating the earliest Prehuman time bin.
*Statistically significant difference ($\alpha = 0.05$).